IAWA Journal, Vol. 22 (2), 2001: 121–131

SHRINKAGE OF THE GELATINOUS LAYER OF POPLAR AND BEECH TENSION WOOD

by

Bruno Clair & Bernard Thibaut

LMGC – Bois, Université Montpellier II, CC 081, Place E. Bataillon, 34095 Montpellier, France
(e-mail: clair@lmgc.univ-montp2.fr)

SUMMARY

Macroscopic longitudinal shrinkage of beech and poplar tension wood is higher than in normal wood. This shrinkage is the result of mechanical interactions of cell wall layers. SEM observation of cut, dried surfaces showed that longitudinal shrinkage is much greater in the gelatinous layer than in other layers. AFM topographic images of the same cells, both in water and in air-dry conditions, confirm this result. Measurements on sections indicate around 4.7% longitudinal shrinkage for the G layer.

Key words: Cell wall, gelatinous layer, shrinkage, tension wood.

INTRODUCTION

Longitudinal shrinkage in wood

Like all other wood properties, hygroexpansion is highly anisotropic. Between the green and ovendry condition, shrinkage ranges from 0.05% to 0.3% in longitudinal, 3% to 6% in radial, and from 6% to 12% in tangential direction (Skaar 1988). According to these values, the hygroexpansion in axial direction is apparently not a problem for the user. However, two cases exist where longitudinal shrinkage is more important: in reaction wood (tension wood of angiosperms and compression wood of gymnosperms) and juvenile wood (Skaar 1988). In these types of wood, axial shrinkage can reach 1% or more (Nepveu 1994). For these woods, shrinkage values cannot be considered as negligible, because wood beams have generally their longer distances in axial direction. These important differences can be explained by the structure of wood fibres.

From wood fibre structure to shrinkage modelling

The knowledge of the woody cell wall, as a multi-layer fibre composite, allows the modelling of the longitudinal shrinkage.

One of the first models, which is still a reference, is the one proposed by Barber and Meylan (1964), refined by Barber (1968). This model considers that the cell wall is reduced to the S_2 layer. The S_2 layer is described as an amorphous hygroscopic matrix in which parallel crystalline microfibrils are imbedded which act to restrain

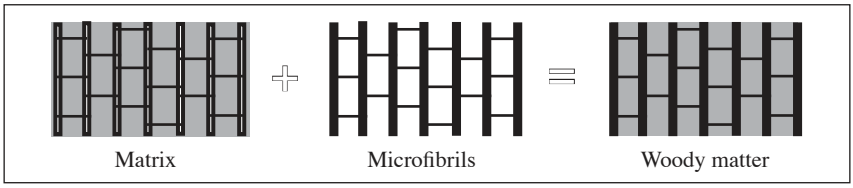

Fig. 1. Schematic representation of the 'reinforced matrix' (Sassus 1998).

hygroexpansion in the direction parallel to their axes (Fig. 1) (Cave 1972a). Thus, microfibril angle is the determinant factor of longitudinal shrinkage. A low angle of microfibril in relation to axial direction induces low axial shrinkage (as in normal wood) and a high angle allows a higher shrinkage (as in juvenile or compression wood). Later, other models integrating other component properties (cellulose, hemicellulose and lignin), changes in matrix behaviour during drying, and introducing the different cell wall layers have been proposed to refine this first model (Barrett et al. 1972; Cave 1972b, 1978; Sassus 1998; Gril et al. 1999; Yamamoto 1999).

These models offer an understanding of macroscopic axial shrinkage for different values of microfibril angle, in normal, compression, and juvenile wood.

However, they cannot explain the behaviour of tension wood, in which the fibre walls have a gelatinous layer. In the G layer, the microfibril angle is very low or nil (Chaffey 2000), even when macroscopic longitudinal shrinkage is high (Clarke 1937; Chow 1946; Sassus 1998). Norberg and Meier (1966) isolated portions of the G layer and did not find a high longitudinal shrinkage. The G layer is generally loosened from the S_2 layer and the latter is very thin in tension wood. So these authors and Boyd (1977) assumed that in tension wood longitudinal shrinkage is caused by the S_1 layer, the G layer being unable to prevent it.

MATERIAL AND METHODS

One poplar tree (*Populus* cv I4551) and one beech tree (*Fagus sylvatica* L.), were chosen for this study. These species are known to have characteristic tension wood with distinct G layers and a high macroscopic axial shrinkage.

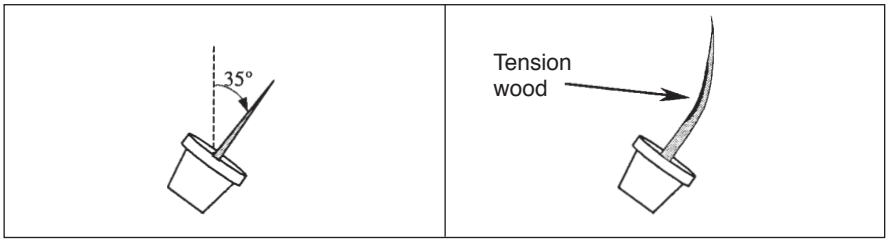

Fig. 2. Recovery of the verticality of a poplar stem after the container had been tilted 35°. Tension wood is produced on the upper side.

Populus cv I4551

During the growing period, a young one-year-old poplar grown in a container was tilted 35° from the vertical. At the end of the growing season, the stem had nearly regained its verticality by producing tension wood on the upper side (Fig. 2). Wood samples were taken from this tension wood zone, showing a large proportion of fibres with G layers and very thin S_2 layers (Fig. 4A).

Fagus sylvatica

A 150-years-old tree was chosen after measurement of peripheral growth stresses at breast height level on the standing tree, on eight positions around the trunk. This tree was typical of a strongly asymmetrical distribution of growth stresses (Fig. 3). A high local level of growth stress is always related to the presence of tension wood (Trénard & Guéneau 1975; Sassus 1994). Wood samples were taken near the highest values of growth stress (Z position on Fig. 3). In spite of thick G layers in the fibre cell walls, the S_2 layer in beech remains thicker than in poplar wood (Fig. 4B).

Wood samples were stored in green condition before further processing into small blocks or thin sections.

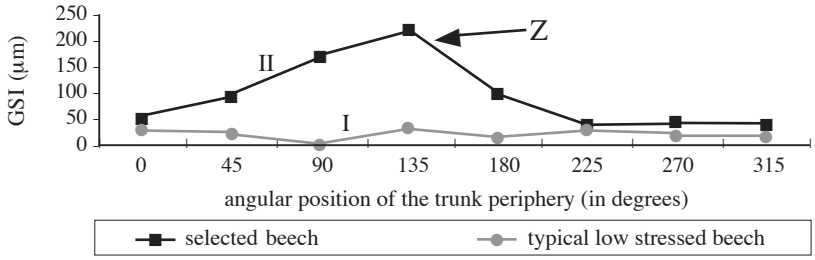

Fig. 3. Growth stress measurement on a standing beech tree, on 8 angular positions of trunk periphery. I: tree with regular low levels of growth stress; II: tree with a zone (Z) of very high tensile growth stress. GSI = Growth Stress Indicator in microns.

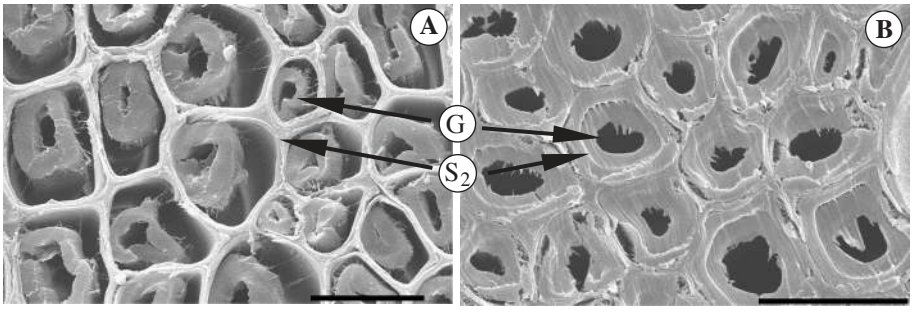

Fig. 4. SEM observation of poplar (A) and beech (B) with a gelatinous layer (G) (also indicated a S_2 layer). — Scale bars: 20 µm.

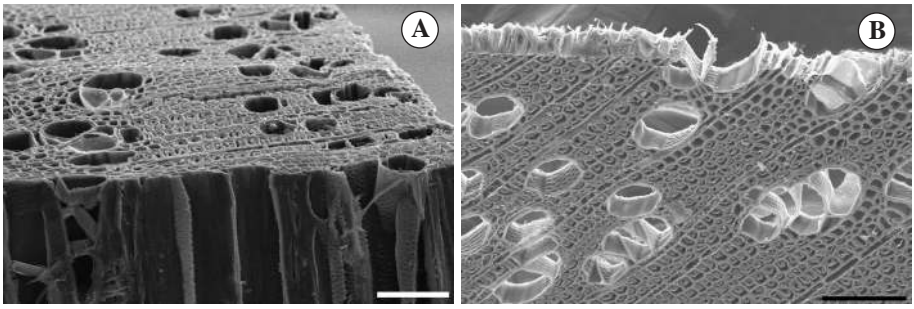

Fig. 5. SEM images of poplar. A: massive block; B: section. — Scale bars: 100 μm.

Massive blocks — Wood sticks (2 cm in longitudinal direction, 5 × 5 mm^2 in cross section) were cut up by splitting in order to guarantee a good axial direction. Sticks were then cut to obtain 5 mm size cubes. Finally a last superficial planing was carried out manually with a new razor blade in order to produce a clean transverse surface, the sample being always kept in a moist condition.

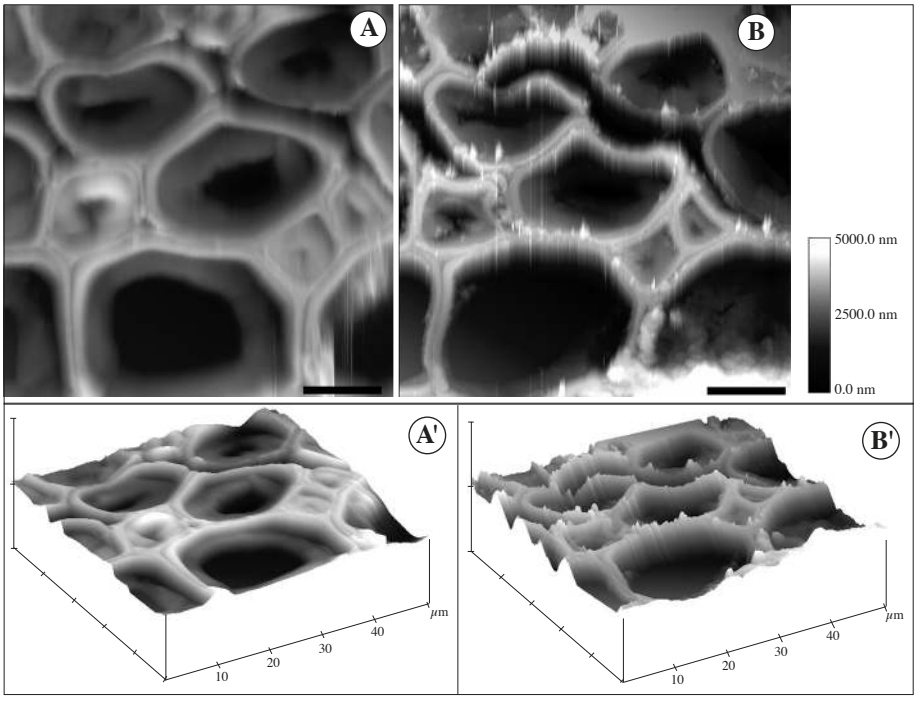

Fig. 6. AFM topographic images of the same cells in water (A, A') and in air-dry condition (B, B'). — Scale bars: 10 μm.

Sections — Transverse sections, 80 μm thick, were cut under water with a microtome equipped with a disposable razor blade. These sections were glued on the specimen stub with the fibre direction parallel to the support, in order to allow observations on transverse surfaces on both sides of the sections.

Scanning electron microscopy

Massive blocks or sections were dehydrated with absolute ethanol, critical point dried, and coated with 300 Å of platinum before observation. Thus, observations were made in ovendry condition with a Cambridge S360 Scan Electron Microscope (Fig. 5).

The tilting of the specimen holder allows observation of the same object from different viewing angles.

Atomic force microscopy

Smaller massive blocks (500 × 500 × 500 μm^3), prepared the same way as before, were observed in transverse view in water and in air-dry condition. Four states were studied: green condition, green condition after two hours in water at 80 °C, air-dry conditions, and wet conditions after air-drying. Atomic Force Microscope (Dimension 3100, Nanoscope IIIa, Digital Instruments) was used to obtain topographic images of a 50 × 50 μm^2 area (around 10 cells). The same cells were observed successively in these conditions (Fig. 6).

RESULTS

Scanning electron microscopy

Massive blocks — Both in poplar and beech individual cells were observed at two angles of view: perpendicular to the surface and then tilted 70° from that direction. From these two images of a single cell, it is possible to draw a topographic profile of the cell after shrinkage (Fig. 8). The x coordinate is given directly by the first image while the y coordinate can be calculated with equation 1 using both images (Fig. 7).

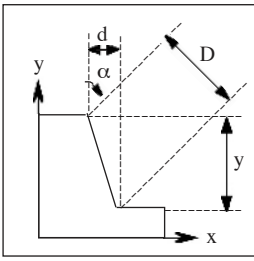

Equation 1:

$$y = \frac{D}{\sin \alpha} - \frac{d}{\tan \alpha}$$

d is the measured distance on the normal image, D on the titled 70° image, and α is 70°

Fig. 7. Principle for calculation of topographic profiles.

These topographic profiles allow measurements of differential shrinkage between cell wall layers. Notably, G layers were far more retracted than other layers (mean 2.2 μm in beech and 2.8 μm in poplar).

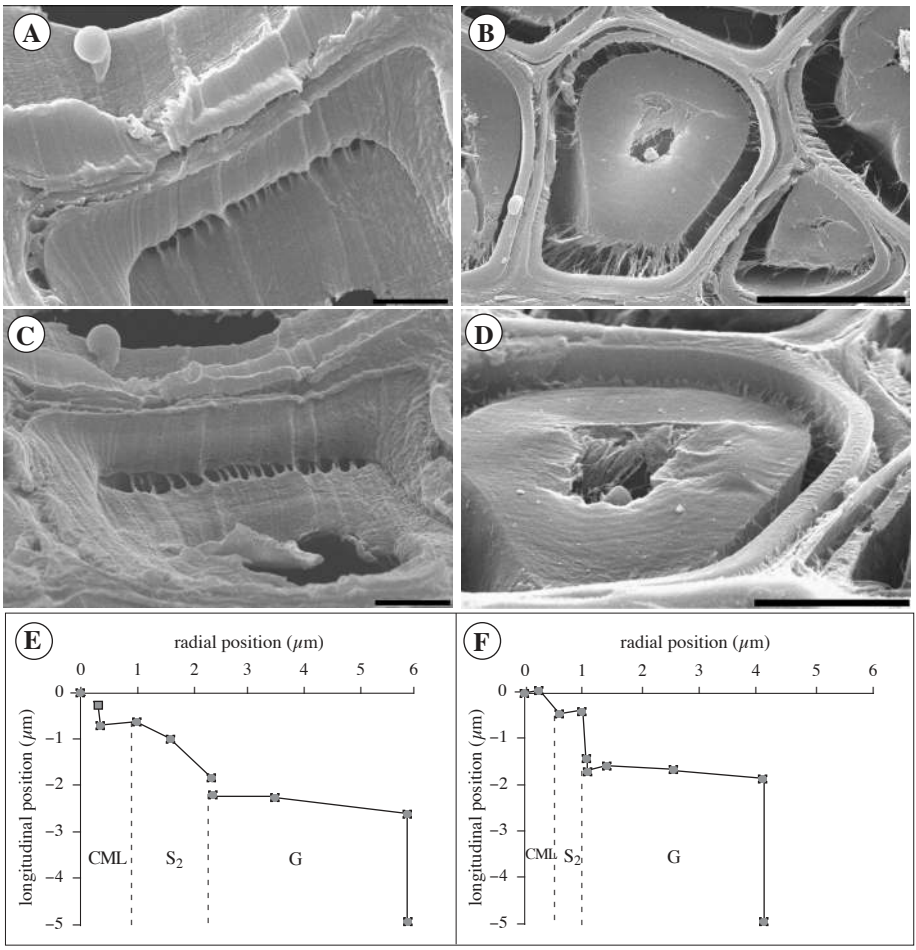

Fig. 8. SEM images and topographic profiles for a single cell of beech (A, C, E) and poplar (B, D, F). A & B: normal to surface images; C & D: at 70° oblique images. — Scale bars: A & C: 2 μm; B: 10 μm; D: 5 μm. CML: compound middle lamella.

In the S_2 layer of beech there seems to be a strain gradient between the S_1 layer and the G layer, which is not the case for poplar.

These observations on massive blocks reveal a differential contraction between cell layers but do not allow a quantitative estimation of actual shrinkage of these layers.

Sections — Several poplar cells were observed after drying. Restraint measurements were made in the same cells in both faces of the section. To this end, numerous images were made at different magnification and viewing angles to locate cells (Fig. 9).

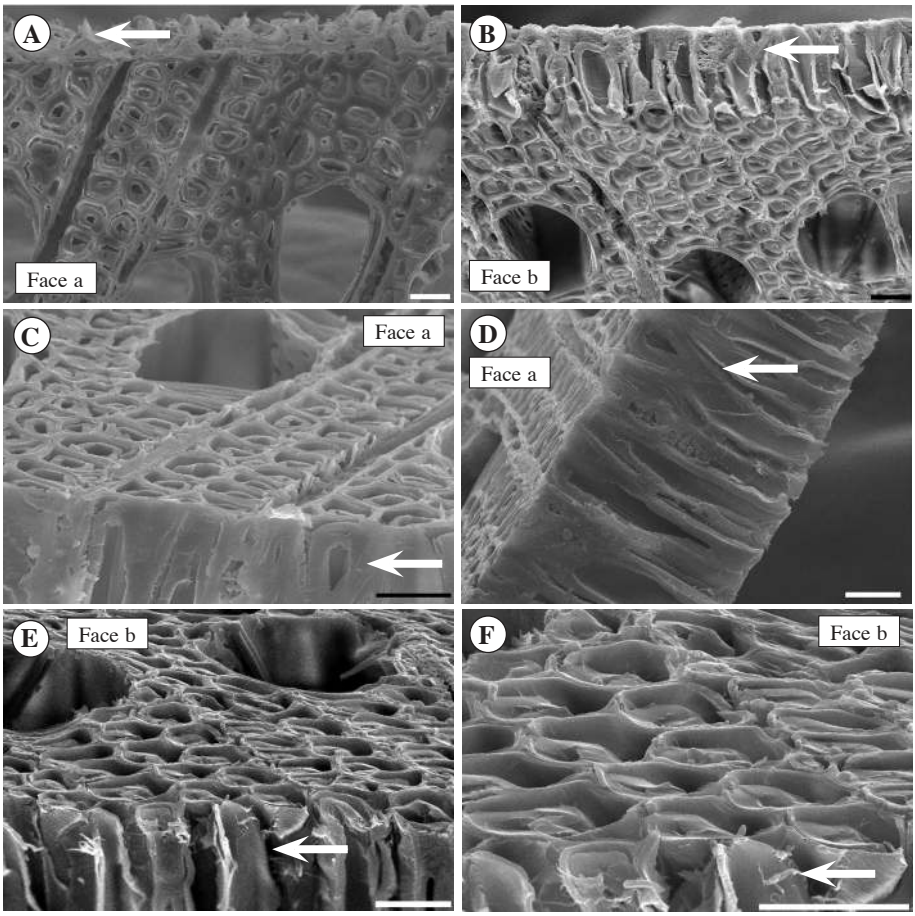

Fig. 9. SEM images of both faces of poplar section with different scales and view angles. Some cells on the edge (arrow) allow the location of other cells. A, C & D: face a; B, E & F: face b. Measurements are made on images like F. — Scale bars: 20 µm.

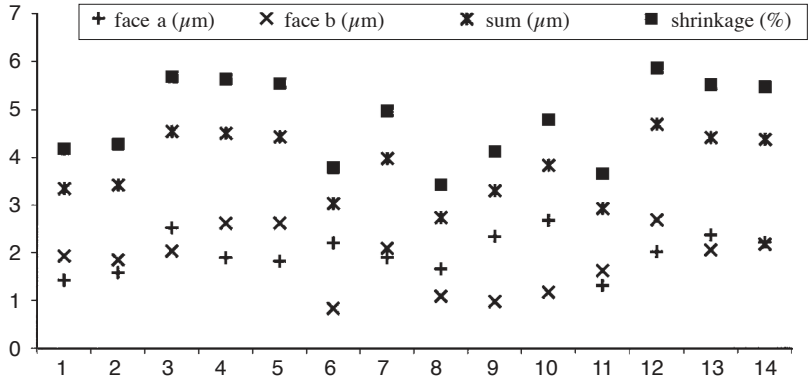

Fig. 10. Differential restraints (µm) and total shrinkage (%) of the G layer for 14 cells.

Results are presented in Figure 10. Mean measurements of differential restraint between G layer and compound middle lamella (CML) are 1.99 μm for one side, 1.83 μm for the other and 3.82 μm for the sum of faces. Thus, the total G-layer differential shrinkage can be estimated from 3.6% to 5.8% with a mean value of 4.7% using the ratio between summation of both restraints and section thickness (80 μm).

Atomic force microscopy

The profile in water (Fig. 11A') shows that there is already a small retraction of the G layer before drying. After two hours in water at 80 °C (Fig. 11B') there is very little additional retraction of the G layer before drying. The profile in the air-dry condition (Fig. 11C') confirms the presence of greater shrinkage in the G layer than in other layers. It was also noted that, after drying, shrinkage in the middle lamella is greater than in the S_2 layer.

The profile in wet conditions after air-drying (Fig. 11D') shows a swelling of the G layer which allows it to almost recover its position in the green condition.

Another profile (not shown), in again air-dry conditions, shows the reversibility of the phenomenon.

DISCUSSION

The first shrinkage observed in water with the AFM method raises questions. It can be explained as a cutting artefact: during cutting, the blade exerts a compression force on the material. Thus, compliant parts (like the middle lamella or S_2 layer) are compressed when the blade is cutting, and stiff parts (like the G layer) are not (or even are pulled up). After the blade has passed, due to recovery of these different stress states, softer and thinner layers lay above stiffer ones like the G layer.

Another explanation can be derived from growth stress release. If the G layer is in a higher tensile stressed state than the other layers, cross-cutting will be the origin of differential strain recovery which is measured here. Anyway, both explanations can be true and generate a cumulative effect.

After drying, a higher differential longitudinal shrinkage can be observed in the G layer. At the same time there is a high transverse shrinkage of this G layer often leading to separation between the G layer and the remaining cell wall.

Again, it can be argued that this separation allows a more complete release of growth stress in the G layer, so that this further differential shrinkage is another expression of growth stress only.

Keeping a sample in hot water (80 °C) during two hours is known as a way to demonstrate viscoelastic and hygrothermal recovery of locked-in strains resulting from growth stresses (Gril & Thibaut 1994). This can be observed only once after a first heating cycle resulting in a contraction or an expansion that can be the reverse of the usual thermal expansion (or sometimes contraction) which is a reversible classical phenomenon (Kübler 1987). In this case, the very low value of measured restraint seems to prove that the viscoelastic recovery, if any, mostly occurred before heating. Thus, hygroscopic shrinkage is the main phenomenon involved.

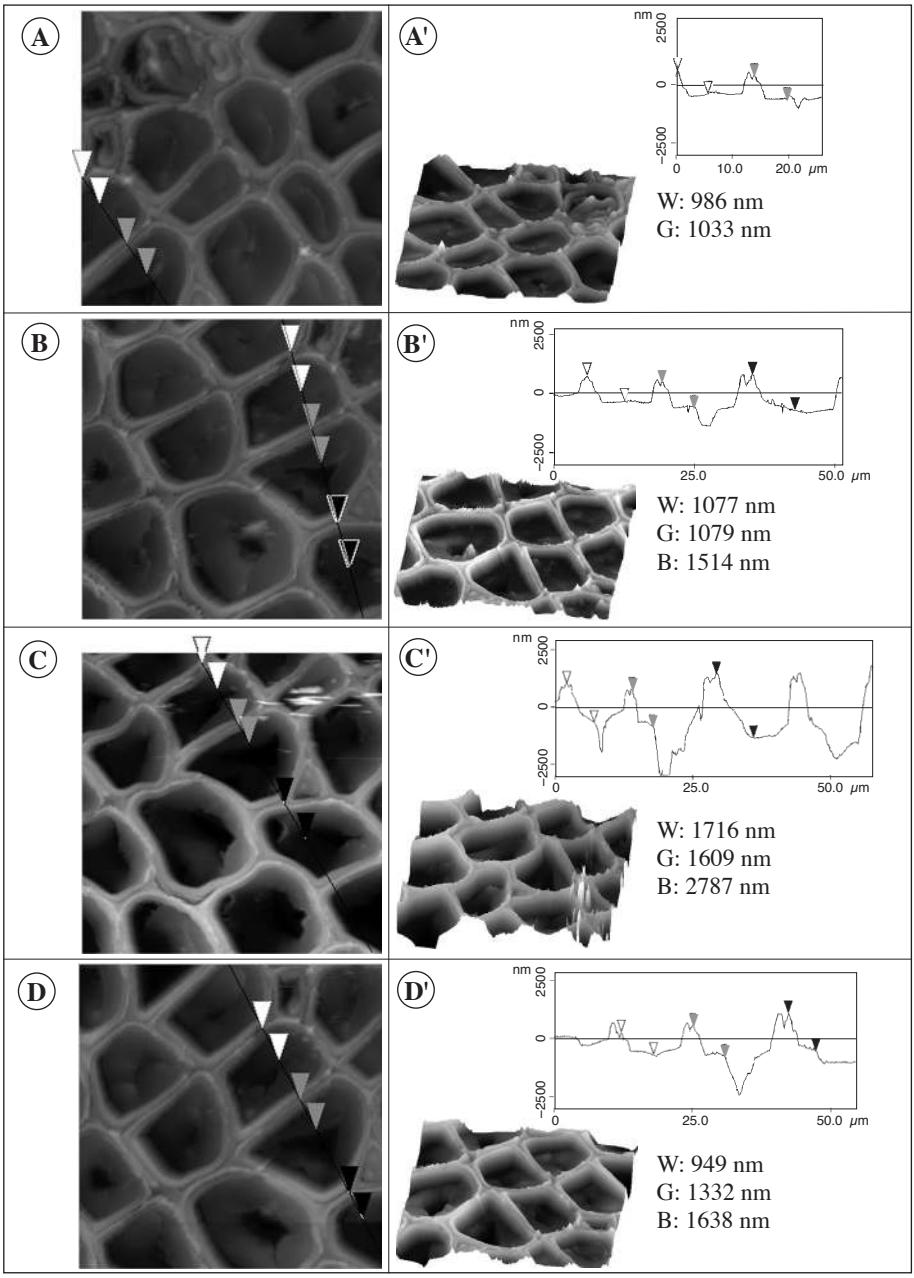

Fig. 11. Measurements on AFM topographic profiles of the same poplar cells in water (A), in water after two hours in hot water of 80 °C (B), in air-dry condition (C), and in water after drying (D). Vertical distance between the S_2 layer and the G layer: W: white cursors; G: grey cursors; B: black cursors.

The swelling of the G layer in water after air-drying confirms the hypothesis of hygroexpansion of the G layer.

Thus, longitudinal shrinkage of the G layer can also be the origin of the strain gradient in the S_2 layer in beech (Fig. 8). During the first drying phases, the G layer is strongly adherent to the S_2 layer and its shrinkage is the origin of high-level drying stresses inside the S_2 layer, inducing a contraction of this layer on the side of the G layer until the layers separate.

These observations of high longitudinal shrinkage in the G layer are contrary to the results of Norberg and Meier (1966), although it is rather difficult to measure strains of a few percent with photographs as these authors did. Thus, G-layer shrinkage, far from being negligible, could be the driving force of high macroscopic longitudinal shrinkage observed in tension wood. Longitudinal shrinkage of the G layer poses a new problem. The G-layer structure, mainly composed of cellulose microfibrils arranged at a very low angle, does not permit to explain this shrinkage with models like the one proposed by Barber (1968).

Even though the fine structure of the G layer is subject to controversy (Norberg & Meier 1966; Côté et al. 1969; Faruya et al. 1970), these observations pose the problem of longitudinal arrangement of the cellulose microfibrils. Longitudinal shrinkage needs the presence of hygro-sensible zones. It seems that these zones, amorphous or disorganised (Yamamoto et al. 2000), would be inserted in crystalline cellulose zones (supposed insensible to humidity changes) both in axial and transverse directions.

CONCLUSIONS

Differential longitudinal shrinkage has been observed and measured on the G layer of beech and poplar tension wood. This study contradicts Norberg and Meier's results. Thus, numerous questions on G-layer structure are raised. Additional studies are needed to understand the mechanisms of shrinkage in the G layer, and to interpret macroscopic shrinkage in tension wood.

ACKNOWLEDGEMENTS

Many thanks are due to Michel Ramonda from the "Service commun de Microscopie en Champ Proche", and to the staff of the "Service commun de Microscopie Electronique", from Université Montpellier 2. We also wish to thank Catherine Coutand from INRA for poplar samples. Frederic Aliotti (student) assisted at the beginning of this study. This study was performed in the framework of the concerted program "wood as a material", funded by ADEME and the French Ministry of Agriculture.

REFERENCES

Barber, N.F. 1968. A theoretical model of shrinking wood. Holzforschung 22: 97–103.

Barber, N.F. & B.A. Meylan. 1964. The anisotropic shrinkage of wood. A theoretical model. Holzforschung 18: 146–156.

Barrett, J.D., A.P. Schniewind & R.L. Taylor. 1972. Theoretical shrinkage model for wood cell wall. Wood Sci. 4: 178–192.

Boyd, J.D. 1977. Relationship between fibre morphology and shrinkage of wood. Wood Sci. & Technol. 11: 3–22.

Cave, I.D. 1972a. Swelling of a fibre reinforced composite in which the matrix is water reactive. Wood Sci. & Technol. 6: 157–161.

Cave, I.D. 1972b. A theory of the shrinkage of wood. Wood Sci. & Technol. 6: 284–292.

Cave, I.D. 1978. Modelling moisture-related mechanical properties of wood. I. Properties of the wood constituents. Wood Sci. & Technol. 12: 75–86.

Chaffey, I. 2000. Microfibril orientation in wood cells: new angles on an old topic. Trends in Plant Sciences 5: 360–362.

Chow, K.Y. 1946. A comparative study of the structure and composition of tension wood in beech (Fagus sylvatica L.). Forestry 20: 62–77.

Clarke, S.H. 1937. The distribution, structure and properties of tension wood in beech (Fagus sylvatica L.). J. Forestry 11: 85–91.

Côté, W.A.J., A.C. Day & T.E. Timell. 1969. A contribution to the ultrastructure of tension wood fibers. Wood Sci. & Technol. 3: 257–271.

Faruya, N., S. Takahashi & H. Miazaki. 1970. The chemical composition of the gelatinous layer from the tension wood of Populus euramericana. J. Jap. Wood Res. Soc. 16: 26–30.

Gril, J., F. Sassus, H. Yamamoto & D. Guitard. 1999. Maturation and drying strain of wood in longitudinal direction: a single-fibre mechanical model. In: G. Nepveu (Ed.), 3rd Workshop on Connection between silviculture and wood quality through modelling approaches and simulation softwares (IUFRO WP S5.01.04 'Biological Improvement of Wood Properties'). ERQB-INRA Nancy, La Londe-Les-Maures: 309–313.

Nepveu, G. 1994. Variabilité. In: A.R. Bo. Lor (Ed.), Le Bois, Matériau d'Ingénierie, Nancy: 127–182.

Norberg, P.H. & H. Meier. 1966. Physical and chemical properties of the gelatinous layer in tension wood fibre of aspen (Populus tremula L.). Holzforschung 20: 174–178.

Sassus, F. 1994. Déformations de maturation et morphologie chez le clone de peuplier 1214. In: B. Thibaut (Ed.), 7ème Séminaire Architecture, Structure et Mécanique de l'Arbre. LMGC, Université Montpellier 2, Montpellier: 159–166.

Sassus, F. 1998. Déformations de maturation et propriétés du bois de tension chez le hêtre et le peuplier: mesures et modèles. Sciences du bois Thesis, ENGREF, Montpellier.

Skaar, C. 1988. Wood-water relations. In: T.E. Timell (Ed.), Springer Series in Wood Science. Springer-Verlag, Berlin, Heidelberg.

Trénard, Y. & P. Guéneau. 1975. Relations entre contraintes de croissance longitudinales et bois de tension dans le hêtre (Fagus sylvatica L.). Holzforschung 29: 217–223.

Yamamoto, H. 1999. A model of anisotropic swelling and shrinking process of wood. I. Generalization of Barber's wood fiber model. Wood Sci. & Technol. 33: 311–325.

Yamamoto, H., N. Soma, T. Okuyama & J. Gril. 2000. Origin of mechanical properties of wood related to the composite structure of the multi-layered cell wall. 3rd Plant Biomechanics Conference. Thieme-Verlag, Badenweiler (Freiburg).